Channel-Like Characteristics of the Low-Affinity Barley Phosphate Transporter PHT1;6 When Expressed in *Xenopus* Oocytes[1][W][OA]

Christian P. Preuss, Chun Y. Huang, Matthew Gilliham, and Stephen D. Tyerman*

Australian Centre for Plant Functional Genomics, Glen Osmond, South Australia 5064, Australia (C.P.P., C.Y.H.); and School of Agriculture, Food, and Wine, University of Adelaide, Glen Osmond, South Australia 5064, Australia (C.P.P., C.Y.H., M.G., S.D.T.)

Remobilization of inorganic phosphate (P_i) within a plant is critical for sustaining growth and seed production under external P_i fluctuation. The barley (*Hordeum vulgare*) transporter HvPHT1;6 has been implicated in P_i remobilization. In this report, we expressed *HvPHT1;6* in *Xenopus laevis* oocytes, allowing detailed characterization of voltage-dependent fluxes and currents induced by HvPHT1;6. HvPHT1;6 increased efflux of P_i near oocyte resting membrane potentials, dependent on external P_i concentration. Time-dependent inward currents were observed when membrane potentials were more negative than −160 mV, which was consistent with nH^+:HPO_4^{2-} ($n > 2$) cotransport, based on simultaneous radiotracer and oocyte voltage clamping, dependent upon P_i concentration gradient and pH. Time- and voltage-dependent inward currents through HvPHT1;6 were also observed for SO_4^{2-}, and to a lesser degree for NO_3^- and Cl^-, but not for malate. Inward and outward currents showed linear dependence on the concentration of external HPO_4^{2-}, similar to low-affinity P_i transport in plant studies. The electrophysiological properties of HvPHT1;6, which locates to the plasma membrane when expressed in onion (*Allium cepa*) epidermal cells, are consistent with its suggested role in the remobilization of P_i in barley plants.

Phosphorus (P) is an essential macronutrient for plant growth and development, being required in the synthesis of nucleic acids, phospholipids, and ATP (Schachtman et al., 1998; Mudge et al., 2002; Lambers et al., 2006). The concentration of inorganic phosphate (P_i) in the cytoplasm of plant cells is maintained at 5 to 17 mM (Schachtman et al., 1998; Mimura, 1999) while it rarely exceeds 10 μM in the soil solution (Goldstein et al., 1988; Mimura, 1999). Agricultural crops heavily rely upon the application of P fertilizers for high yields (Morgan, 1997; Shenoy and Kalagudi, 2005; Lambers et al., 2006). P fertilizers are produced from nonrenewable deposits, and they are predicted to be half-depleted within 50 to 70 years (Oelkers and Valsami-Jones, 2008). Repeated application of P fertilizers can also result in significant environmental pollution (Sharpley et al., 1994; Molen et al., 1997).

The most promising way to reduce the dependence upon P fertilizers is to improve crop P use efficiency (Graham and Welch, 1996; Shenoy and Kalagudi, 2005). This may be achieved by increasing P_i uptake or increasing the efficiency of P_i remobilization within the plant (Shenoy and Kalagudi, 2005). Remobilization of P_i is considered as an extremely important strategy for plant productivity in the environments where there is a large fluctuation in P_i supply (Papakosta, 1994; Rae et al., 2003). P_i remobilization is required for root growth under P_i-limiting environments (Marschner et al., 1996; Jeschke et al., 1997), and therefore affects root P_i uptake capacity (Shin et al., 2006), acting as a negative feedback control mechanism (Drew and Saker, 1984; Marschner et al., 1996; Peng and Li, 2005). P_i remobilization from older/shaded leaves also allows continued growth of younger and more photosynthetically active leaves (Jeschke et al., 1997), and it accounts for the majority, if not all of the P found in cereal grains (Horst et al., 1996; Masoni et al., 2007). Plant P_i transporters are involved in the movement of P_i within the cell and around the plant, and have been separated into families based on their predicted membrane localization: PHT1 (plasma membrane), PHT2 (plastid inner envelope), PHT3 (mitochondrial inner membrane), PHT4 (chloroplasts, heterotrophic plastids, and Golgi), and pPT (plastid inner envelope; Guo et al., 2008).

Plasma membrane P_i transporters (PHT1) are characterized as either high or low affinity and play a critical role in P_i movement between cells or tissues (Rae et al., 2003). Although much is known about high-affinity P_i transporters involved in P_i uptake by roots, little is currently known about the P_i transporters involved in remobilization.

[1] This work was supported by the F.J. Sandoz Scholarship, the University of Adelaide, the Australian Research Council, the Grains Research and Development Corporation, and the South Australian Government.

* Corresponding author; e-mail steve.tyerman@adelaide.edu.au.

The author responsible for distribution of materials integral to the findings presented in this article in accordance with the policy described in the Instructions for Authors (www.plantphysiol.org) is: Stephen D. Tyerman (steve.tyerman@adelaide.edu.au).

[W] The online version of this article contains Web-only data.

[OA] Open Access articles can be viewed online without a subscription.

www.plantphysiol.org/cgi/doi/10.1104/pp.109.152009

The P_i transporter *HvPHT1;6* is highly expressed in old leaves compared to young leaves, and its transcript is abundant in phloem tissue, with a lower level also observed in mesophyll cells (Rae et al., 2003). The expression of *HvPHT1;6* in both shoots and roots is upregulated by P deficiency, and *HvPHT1;6* is the only *HvPHT1* family member found so far that is expressed in the shoots with high abundance (Rae et al., 2003; Huang et al., 2008). In addition, overexpression of *HvPHT1;6* in rice (*Oryza sativa*) suspension cells suggests it may have a high K_m or linear uptake kinetics (above wild-type P_i transport) to 1 mM external P_i (Supplemental Material S1). These data suggest that *HvPHT1;6* plays a major role in P_i remobilization.

Until recently, heterologous expression of plant P_i transporters in yeast (*Saccharomyces cerevisiae*) mutants lacking high-affinity P_i transporters (Pho84 and Pho89) have been the main means for functional characterization of both high- and low-affinity plant P_i transporters (Muchhal et al., 1996; Leggewie et al., 1997; Daram et al., 1998; Guo et al., 2008; Liu et al., 2008). In two cases, plant suspension cells have been used for functional characterization of plant P_i transporters (Mitsukawa et al., 1997; Rae et al., 2003); however, detailed electrophysiology has not been performed. It is difficult to perform electrophysiological measurements in yeast, as well as to isolate specific plant cell types for electrophysiological measurements. *Xenopus laevis* oocytes have been used for characterization of various P_i transporters including mammalian sodium (Na)-Pi cotransporters and a plant P_i transporter (Bacconi et al., 2005; Ai et al., 2009). The rice phosphate transporter OsPT2 failed to complement yeast with a defect in high-affinity P_i transporters, but when expressed in *X. laevis* oocytes membrane depolarization could be observed in the presence of PO_4^{2-} (Ai et al., 2009). However, voltage dependence of proposed P_i transport, or potential interactions with other ions, was not investigated.

In this study, we confirm a plasma membrane localization of HvPHT1;6, and present a comprehensive analysis of HvPHT1;6 transport activities using the *X. laevis* oocyte expression system. Our results demonstrate that HvPHT1;6 is most likely to be a proton-coupled P_i transporter, though it has time-dependent activation at negative membrane potentials with linear concentration dependence similar to voltage-dependent ion channels; it also appears to transport SO_4^{2-} coupled to protons. As such, we discuss our results in the context of the proposed role of HvPHT1;6 in P_i and sulfur (S) remobilization within the plant.

RESULTS

Plasma Membrane Localization of HvPHT1;6

HvPHT1;6 mediates P_i transport into rice suspension cells (Rae et al., 2003), but its plasma membrane localization has not been established. Therefore, we created a *HvPHT1;6::GFP* construct and transiently coexpressed with either the plasma membrane targeted marker, *AtPIP2A::mCherry*, or the vacuolar membrane marker, *γTIP::mCherry* (Nelson et al., 2007), in onion (*Allium cepa*) epidermal cells. The green fluorescence of HvPHT1;6::GFP (Fig. 1B) colocalized with the red fluorescence of the plasma membrane marker pmrk (Fig. 1, C and D). In addition, the cellular location of the green fluorescence of HvPHT1;6::GFP (Fig. 1F) was separated from that of the red fluorescence of the vacuolar marker (Fig. 1, G and H), under hypertonic treatment. The red fluorescence of the vacuolar membrane marker was slightly intracellular compared to the green fluorescence of HvPHT1;6::GFP (Fig. 1H). These results indicate that HvPHT1;6 is located on the plasma membrane.

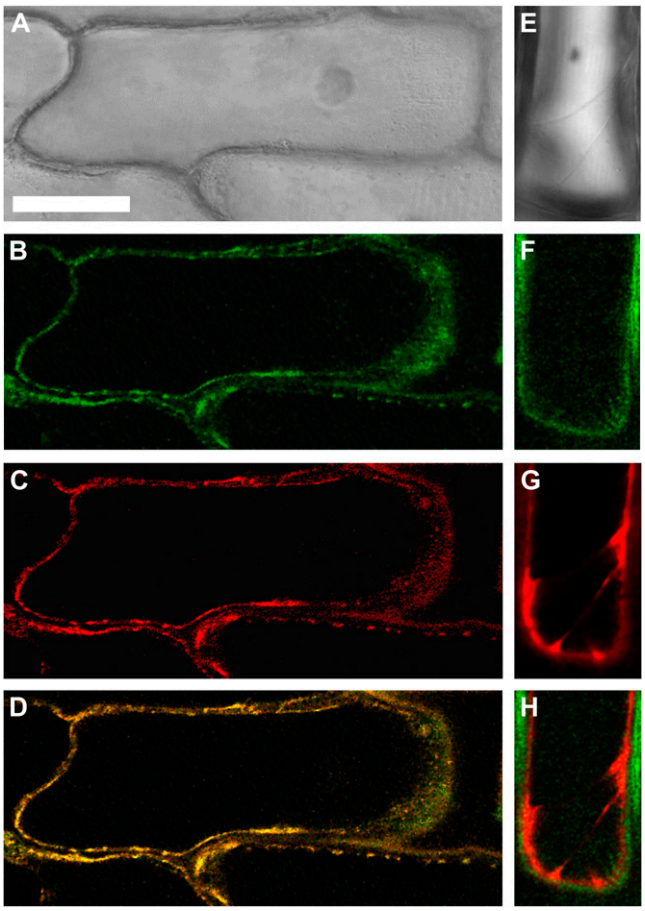

Figure 1. Intracellular localization of HvPHT1;6. A, Bright-field image of onion epidermal cells. B, The intracellular localization of HvPHT1;6::GFP in onion epidermal cells. C, The intracellular localization of the plasma membrane marker, AtPIP2A::mCherry. D, Overlay of HvPHT1;6::GFP and AtPIP2A::mCherry; colocalization shown in yellow. E, Bright-field image of a second onion epidermal cell. F, The intracellular localization of HvPHT1;6::GFP in this cell. G, The intracellular localization of the vacuolar membrane marker, γTIP::mCherry fusion. H, Overlay of the HvPHT1;6::GFP and γTIP::mCherry fusion, showing differing localization of green and red fluorescence. Bar = 100 μm.

Effects of HvPHT1;6 on Mortality of *X. laevis* Oocytes

Injection of *HvPHT1;6* cRNA into *X. laevis* oocytes resulted in a 2-fold increase in oocyte deaths relative to water-injected control oocytes over the same time when incubated in modified Barth's solution (MBS; Fig. 2A). Addition of 1 mM or 10 mM P_i to the MBS solution significantly decreased mortality of *HvPHT1;6* cRNA-injected oocytes (Fig. 2A). No such relationship was observed in water-injected oocytes, nor for the positive control, oocytes expressing a human Na-P_i transporter. This human Na-P_i transporter has previously been shown to transport P_i into oocytes coupled with the downhill influx of Na^+ (Bacconi et al., 2005; Virkki et al., 2005), and we are also able to show its electrogenic P_i transport activity (data not shown). *HvPHT1;6*-injected oocytes also had a higher efflux rate of P_i compared to controls when no P_i was added to the bath solution (Fig. 2B). This difference in efflux was abolished when 10 mM external P_i was applied (Fig. 2B), which was correlated with the reduced mortality of *HvPHT1;6*-injected oocytes incubated in MBS + 10 mM P_i (Fig. 2A). The application of P_i to the bath solution reduces free Ca^{2+} concentrations, which could have an impact on oocyte mortality. To discount this possibility we examined the effect of addition of 0.5 mM and 2 mM external calcium. There was no significant difference in oocyte survival or transport current ($P > 0.7$ for each test, $n = 10$). These results suggest that the increased death rate in *HvPHT1;6*-injected oocytes is due to the enhanced P_i efflux.

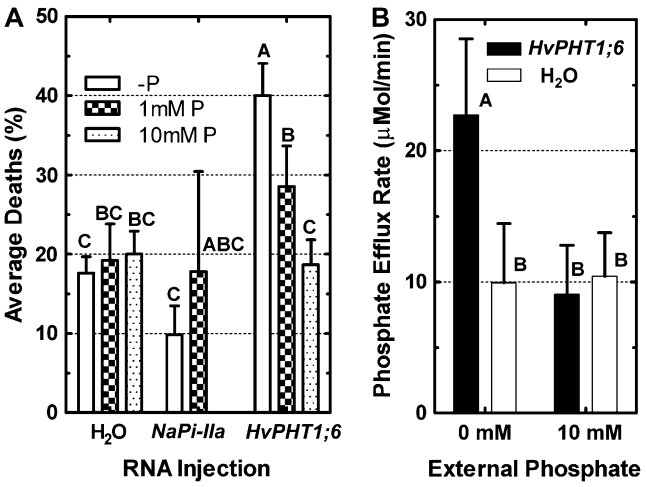

Figure 2. External phosphate reduces death of *HvPHT1;6* cRNA-injected oocytes. A, Percentage of oocyte deaths incubated in pH 7.5 MBS, containing three P_i (P) concentrations (KH_2PO_4), over 3 to 5 d at 18°C. Columns are means of three to eight replicates. B, $H_3{}^{32}PO_4$ efflux rate. Oocytes were incubated for 24 h in MBS buffer with 10 mM 850 cpm nmol^{-1} P_i before measuring the efflux rate in MBS over time. Data were corrected for radioactivity in wash solution. Standard errors ($n = 4$) are shown as vertical bars. Different letters indicate a significance difference at $P_{0.05}$ for confidence interval.

Time- and Voltage-Dependent Inward Currents Induced by HvPHT1;6

A bath solution containing 100 mM Cl^- (ND-100) was used for characterization of mammalian P_i transporters in *X. laevis* oocytes (Bacconi et al., 2005). Large inward currents were detected in *HvPHT1;6*-injected oocytes when ND-100 was used as a bath solution (data not shown). Water-injected control or cRNA-injected oocytes in solutions containing low amounts of Cl^- had a much lower inward current. Therefore, we used a 10 mM NaCl base solution (ND-10) generally (see "Materials and Methods") to which anions were balanced with *N*-methyl-D-glucamine (NMDG).

Under two-electrode voltage clamp (TEVC), negative-going voltage pulses caused the activation of a time- and voltage-dependent inward current that was increased by adding external P_i and was not observed in water-injected control oocytes (Fig. 3A). The example shown in Figure 3A is for 1,2-bis(2-aminophenoxy)ethane-*N*,*N*,*N*′,*N*′-tetraacetic acid (BAPTA)-injected HvPHT1;6-expressing oocytes bathed in a modified ND-10 with Ba^{2+} replacing Ca^{2+} (Fig. 3A). Ba^{2+} and BAPTA were used to circumvent possible disturbance to the cytosolic Ca^{2+} concentration potentially caused by HvPHT1;6 expression as such changes in cytosolic Ca^{2+} concentration could elicit native oocyte inward currents (Weber et al., 1995). HvPHT1;6-induced currents in these conditions were statistically the same as in non-BAPTA-injected oocytes ($P > 0.7$), and those in calcium-bath solutions ($P = 0.5$). Therefore, these treatments were not used for the majority of the following experiments. The activation of known endogenous oocyte channels was compared with that induced by *HvPHT1;6* cRNA injection (Supplemental Material S2). HvPHT1;6 expression elicits currents different from native channels identified in the literature. Closer inspection of currents at less-hyperpolarized voltages with 10 mM P_i, $SO_4{}^{2-}$, or $NO_3{}^-$ in the bath solution revealed that steady-state inward currents began to be significantly activated at voltages more negative than about −90 mV (when voltage was held constant for 4.5 s; Fig. 3).

When the voltage was taken to less-negative values after fully activating the inward current at −150 mV, the current deactivated to a steady level with a half-time of 0.33 ± 0.05 s (Fig. 3B). The difference in current between the initial and steady-state value during deactivation provides the time-dependent component of the *HvPHT1;6* cRNA-induced current at various voltages. We refer to this as the tail current. The majority of the following figures show results obtained from such tail analysis.

Gradient-Dependent Currents and Fluxes

To further examine the effect of altering the gradient of P_i across the plasma membrane on the HvPHT1;6-induced tail currents, we injected water or P_i into *HvPHT1;6*-injected oocytes to a final calculated concentration of 10 mM and compared this with water-

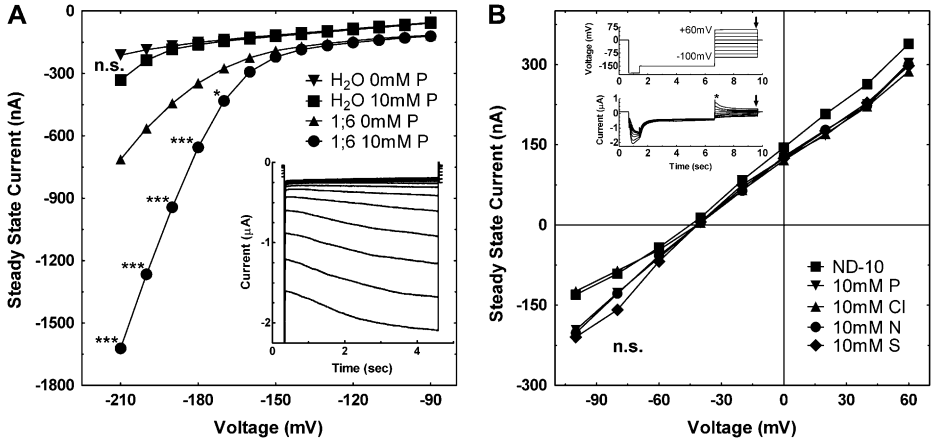

Figure 3. *HvPHT1;6*-cRNA injection-induced inward current at hyperpolarized membrane potentials. A, Current/voltage curves of *HvPHT1;6*-cRNA, and water-injected oocytes. Oocytes were also BAPTA injected and bathed in ND-10 with Ba^{2+} replacing Ca^{2+} (pH 7.5). Values are the most negative current from a 4.2 s voltage hold (−90 to −210 mV in 10 mV increments). Data points are means of eight oocytes. Asterisks indicate a significant difference using Tukey's test ($P_{0.05}$ or $P_{0.001}$) between currents induced in 0 and 10 mM external NMDG-phosphate concentration. The inset shows overlayed current versus time traces at each voltage of *HvPHT1;6* cRNA-injected oocytes bathed in 10 mM P_i. B, Steady-state current/voltage curves extracted from tail current end point (arrows in the inset) comparing different external anions on *HvPHT1;6*-injected oocytes in ND-10, pH 7.5. Data points are means of at least five oocytes, no significant difference (n.s.) was observed ($P_{0.05}$). Inset shows voltage protocol and example tail current trace overlay. Arrows indicate the tail end point, while currents marked at the asterisk time point are subtracted from the end point for tail current/voltage curves. P, Phosphate; Cl, chloride; N, nitrate; S, sulfate.

injected oocytes, bathed in either 0 or 10 mM P_i added to ND-10. The largest inward tail currents at negative voltages were obtained when there was the largest gradient for inward movement of P_i (0 P_i injected, 10 mM P_i in bath; Fig. 4A). Inward tail currents were smallest when this gradient was reversed (10 mM P_i injected, 0 P_i added to bath; Fig. 4). With 10 mM P_i injected and 10 mM in the bath, the tail current/voltage curve reversed at 0 mV (Fig. 4A) under these conditions where the bath pH was 7.5. We measured ^{32}P uptake into *HvPHT1;6*-injected and control oocytes with voltage clamped at −130 mV for 7.5 min (Fig. 4B). The influx was increased 22-fold above that measured in control oocytes, and corresponded to a similar increase in the amount of charge that moved into the oocyte (Fig. 4B). Therefore, the currents associated with P_i influx were accompanied by a flow of net-positive charge inwards to the oocyte. The same phenomenon was observed when ^{35}S was applied (Fig. 7B).

Concentration Dependence and Selectivity

HvPHT1;6-injected oocytes showed a significant P_i-induced increase in both inward and outward tail currents (Fig. 5). Corresponding with this was a small but significant shift in reversal potential toward positive voltages. The mean tail current as a function of added P_i in the bath was linear in the range of external P_i concentrations tested (Fig. 4B). Note that for a simple anion channel response it would be expected that the reversal potential would shift negative with increasing P_i inward directed gradient (see also Fig. 4).

Selectivity of HvPHT1;6-induced currents to different anions was investigated by measuring steady-state currents at −150 mV (Fig. 6A), a physiologically relevant resting membrane potential for plant cells. The selectivity at −150 mV was $HPO_4^{2-} > SO_4^{2-} > NO_3^- > Cl^-$, where the external free anion concentration applied was kept constant at 9.9 mM (calculated using Visual MINTEQ, Royal Institute of Technology, Sweden). The organic anions, malate and citrate were also tested, but *HvPHT1;6*-injected oocytes showed no significant transport of these two organic anions over water-injected controls ($P > 0.8$; data not shown). Bis-Tris propane (BTP) control solution induced less inward current than ND-10, which could be due to residual chloride transport through HvPHT1;6 in ND-10. Also slight but significantly higher currents were seen in water-injected oocytes in the BTP solution (as opposed to the ND-10-based solutions), presumably due to a large difference in chloride concentration between the internal oocyte (24–62 mM; Weber, 1999) and the external bath (0.6 mM). When tail currents were measured at less-negative membrane potentials (Fig. 6B) SO_4^{2-} and P_i gave equal inward currents, and NO_3^- and Cl^- gave smaller and similar currents. However, NO_3^- gave larger outward tail currents than any other anion (Fig. 6B). No significant anion-induced tail currents were observed in water-injected controls (inset in Fig. 6B).

A P_i and SO_4^{2-} competition experiment was performed to examine if competition occurred for transport sites of HvPHT1;6 between these two anions (Fig. 7A); the inward and outward tail currents were com-

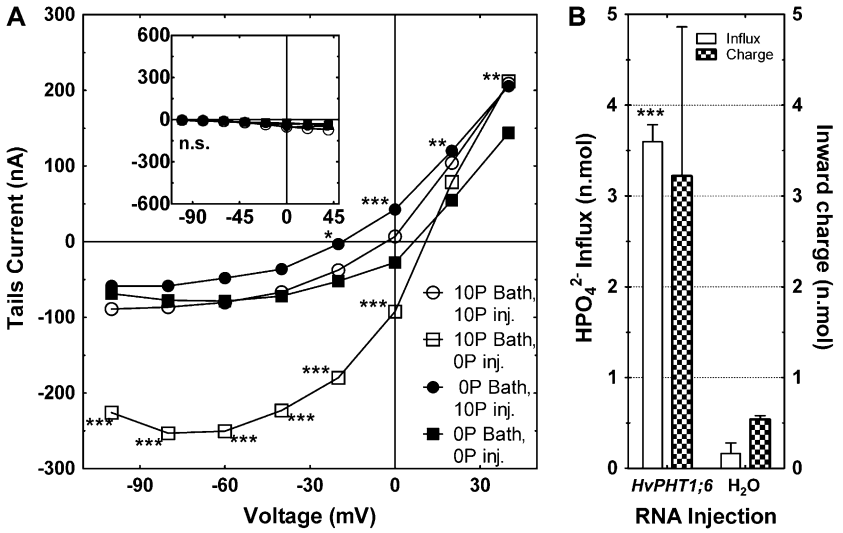

Figure 4. HvPHT1;6-induced phosphate transport is cation coupled. A, Tail current/voltage analysis of *HvPHT1;6* cRNA-injected oocytes in response to 0 or 10 mM NMDG-phosphate in the pH 7.5 ND-10 bath solution combined with 0 or 10 mM or internal oocyte NMDG-phosphate at least 2 h after injection. The inset shows water-injected oocyte controls. n.s., No significant difference. B, The average current integrals and subsequent radioactive $H_3{}^{32}PO_4$ influx with a 450 s long hold at −130 mV in a nonflowing pH 7.5 ND-10 bath solution. Data points in each experiment represent means of four to eight oocytes. Error bars indicate SEM, and asterisks denote a significant difference using the Scheffe's test ($P_{0.05,\ 0.01,\ 0.001}$).

pletely additive between the two anions. Plotting the currents against the sum of the anions (HPO_4^{2-} + SO_4^{2-}) displayed a linear relationship (inset in Fig. 7A) with mean R^2 values ranging from 0.97 to 1.00 across all voltages.

External pH Sensitivity

We examined the external pH (pH_o) sensitivity of tail currents in P_i and SO_4^{2-} containing solutions, and no significant pH_o effect was detected in water-injected controls. Figure 8A shows that an increase in bath protons (pH decrease from pH 8 to 6) significantly increases the currents predicted to be SO_4^{2-} influx. The change in current was linear over this pH range, increasing by a factor of 2.02 ± 0.18 per pH unit. In contrast, *HvPHT1;6*-injected oocytes showed the largest P_i-induced inward currents at pH 7.5 (Fig. 8B). The general trend for P_i transport therefore opposes what was seen for SO_4^{2-}. However, the HPO_4^{2-} ion is predicted to decrease in free concentration as pH decreases (calculated using Visual MINTEQ). If we take account of the stimulating effect of lower pH on SO_4^{2-} currents, and make the assumption that the selectivity between HPO_4^{2-} and SO_4^{2-} does not change with pH, we can calculate predicted inward currents for HPO_4^{2-} as a function of pH (Fig. 8B). Within the confidence limits of the measured currents, the predicted currents fit reasonably well with HPO_4^{2-} being the transported form of P_i.

DISCUSSION

Despite the importance of low-affinity P_i transporters in P_i remobilization in higher plants, the functional characterization of low-affinity P_i transporters from plants has been limited to either the complementation of yeast mutants defective in high-affinity P_i permeases (Daram et al., 1998; Miller and Zhou, 2000; Guo et al., 2008; Liu et al., 2008) or ectopic expression of low-affinity P_i transporters in rice (Rae et al., 2003) or tobacco (*Nicotiana tabacum*; Mitsukawa et al., 1997) suspension cells. One study in *X. laevis*

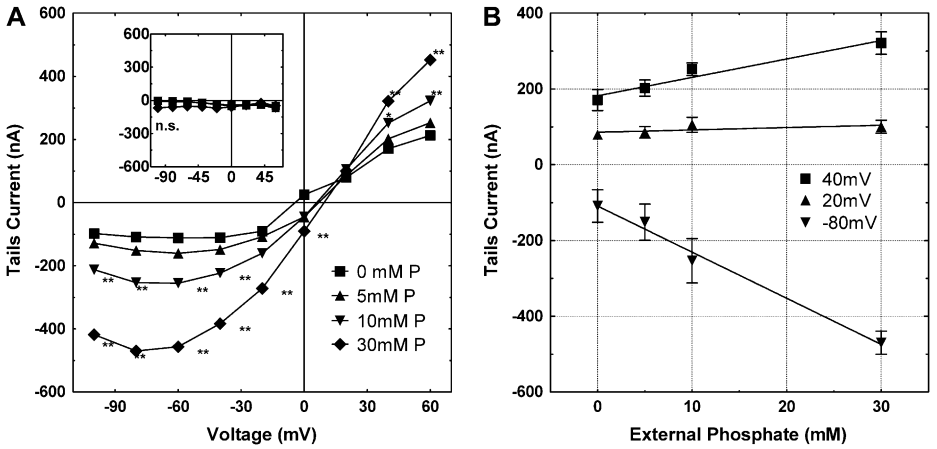

Figure 5. HvPHT1;6 transports phosphate with low affinity. A, Current/voltage tail plot of *HvPHT1;6*-injected oocytes bathed in ND-10 with different phosphate concentrations at pH 7.5. The inset shows water-injected oocyte responses. n.s., No significant difference. Asterisks indicate a significant difference at $P_{0.05}$ and $P_{0.01}$ using Tukey's test. B, *HvPHT1;6*-injected oocyte tail analysis at selected voltages. Error bars indicate SEM of four oocytes.

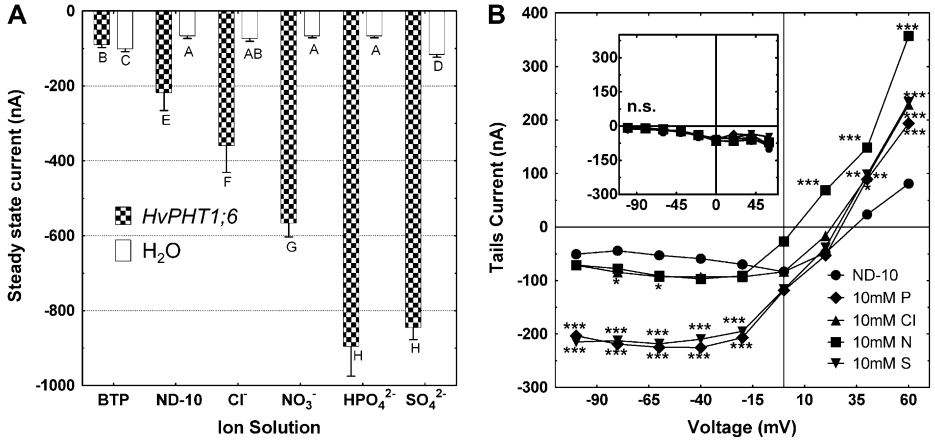

Figure 6. Anion selectivity of HvPHT1;6. A, Steady-state current response to six different bath solutions: BTP control, ND-10 control, ND-10 plus 9.9 mM transported oxyanion (actual applications were 10 mM), NMDG-chloride (Cl^-), 10 mM NMDG-nitrate (NO_3), 14.88 mM NMDG-phosphate (HPO_4^{2-}), or 11 mM NMDG-sulfate (SO_4^{-2}). Steady-state currents were recorded after 5 s at −150 mV. Columns represent means of five oocytes, and error bars indicate SEM. Different letters indicate significant differences at $P_{0.05}$ via confidence interval. B, Tail current/voltage responses of *HvPHT1;6*-injected and water-injected oocytes run in a ND-10 bath (control), or containing either NMDG-phosphate (P), NMDG-chloride (Cl), NMDG-nitrate (N), or NMDG-sulfate (S). pH was buffered with Tris-base to pH 7.5. The inset shows the response of water-injected controls. n.s., No significant difference. Asterisks indicate a significant difference at $P_{0.05,\ 0.01,\ 0.001}$ (Tukey's test) between the respective anion treatment and the control.

oocytes of a plant P_i transporter (OsPHT1;2) shows only limited information on membrane depolarizations when 1 or 10 mM NaH_2PO_4 was applied, suggesting that OsPHT1;2 is a low-affinity P_i transporter (Ai et al., 2009).

We first show that HvPHT1;6 is expressed in the plasma membrane of plant cells (Fig. 1), secondly that HvPHT1;6 expression is not just activating a known native transporter in the plasma membrane of *X. laevis* oocytes (Supplemental Material S2). This information gives relevance to HvPHT1;6 being involved in P_i movement between plant cells/tissues and that characterization in *X. laevis* oocytes is appropriate.

Expression of the low-affinity HvPHT1;6 transporter in *X. laevis* oocytes with no supplementation of P_i in the external medium caused increased deaths of the oocytes (Fig. 2A). Based on $^{32}P_i$ efflux measurements (Fig. 2B) we interpret the increased deaths of the oocytes as a result of increased P_i efflux caused by expression of HvPHT1;6. The resting membrane potential for *HvPHT1;6*-injected oocytes in ND-100 solution was −26.8 ± 2.6 mV that is not different from the

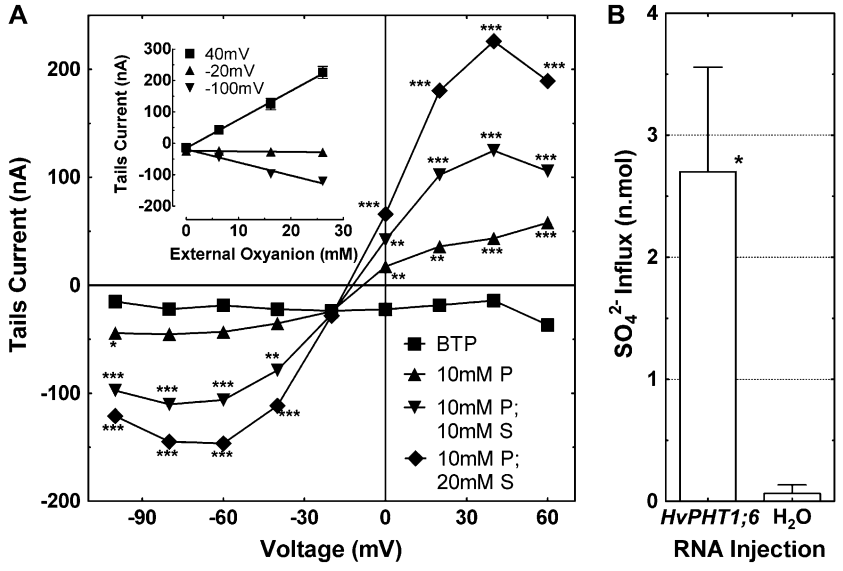

Figure 7. Phosphate and sulfate competition. A, Tail current/voltage plot of *HvPHT1;6*-injected oocytes between the BTP control solution, and the BTP containing 10 mM H_3PO_4 (P) with or without 10 or 20 mM H_2SO_4 (S). pH was buffered with Tris-base to pH 7.5. The inset shows a linear regression of selected currents against calculated free HPO_4^{2-} or SO_4^{2-} in the bath solution ($r^2 > 0.96$, Visual MINTEQ). Data points indicate means of seven individual oocyte measurements. B, Radioactive $Na_2{}^{35}SO_4$ influx with a 450 s long hold at −130 mV in a stagnant pH 7.5 ND-10 bath solution. Columns are means of five oocytes. Error bars indicate SEM, and asterisks denote a significant difference using Tukey's test ($P_{0.05,\ 0.01,\ 0.001}$).

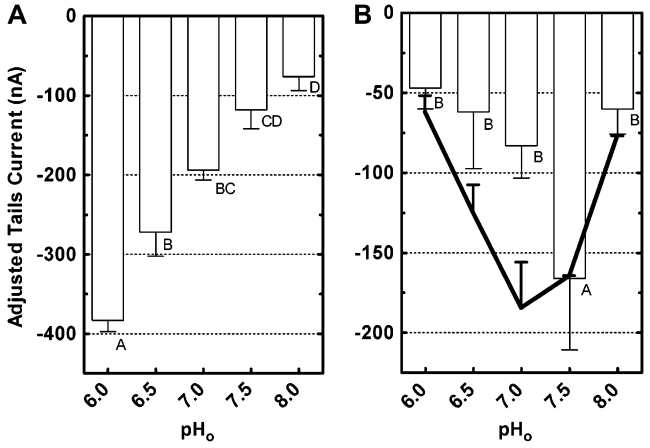

Figure 8. Proton-coupled P_i transport activity of HvPHT1;6. HvPHT1;6-induced outward and inward currents in response to sulfate (A) or phosphate (B). Columns indicate mean currents of eight oocytes for phosphate transport via HvPHT1;6 only, using a dual subtraction process: (1) subtracting water-injected oocyte currents from HvPHT1;6 injected, then (2) subtracting ND-10 control solution currents from ND-10 plus 10 mM NMDG-phosphate or sulfate currents at each pH_o. Letters indicate significant difference ($P_{0.05}$, Tukey's test), and error bars represent SEM. Predicted HPO_4^{2-} currents (solid line in B) accounting for changes in [HPO_4^{2-}] with pH_o were calculated from the SO_4^{2-} currents assuming that the transport selectivity between HPO_4^{2-} and SO_4^{2-} does not change with pH_o. Predictions are only given for influx because accurate estimation of internal oocyte activity of HPO_4^{2-} and SO_4^{2-} could not be made.

resting membrane potential in MBS of -29.2 ± 9.5 mV, this could be a reason why P_i efflux occurs in the absence of external P_i. Data in Figure 4A show that under conditions of high internal P_i, and with zero in the bath, the reversal potential of *HvPHT1;6*-injected oocytes, as indicated by tail currents, is close to these values. When P_i is added to the bath, the reversal potential shifts positive, which we predict would reduce P_i efflux from the oocyte (see below for more discussion in "Stoichiometry of H^+-P_i Cotransport and Speciation"). In plant cells, efflux of P_i through HvPHT1;6 under membrane depolarization could be related to efflux of P_i from leaf mesophyll cells when they start senescing, and is possibly why enhanced expression is seen in older leaf mesophyll cells (Rae et al., 2003). However, this would require neutral to alkaline pHs in the external medium as used in our oocyte experiments.

Voltage Dependence

Activation of inward current in *HvPHT1;6*-injected oocytes occurred when voltages were more negative than −60 mV, and became highly significant between −130 and −160 mV (Fig. 3). This is a rather novel finding, but is not totally unexpected, because while the resting potential of an oocyte is usually around −30 to −40 mV, the equivalent value for a plant cell can be less than −200 mV (Dreyer et al., 1999), and phloem cells are more hyperpolarized than their surrounding cells (Hafke et al., 2005). The hyperpolarization in phloem cells should be able to activate HvPHT1;6 to facilitate P_i loading in phloem-associated cells for future remobilization. In many respects the slow kinetics of voltage activation of HvPHT1;6 observed in oocytes is similar to some plant ion channels (Marten et al., 1999). The linear concentration transport kinetics would further support that HvPHT1;6 possesses characteristics of an ion channel. However, the evidence that inward current corresponds to anion influx instead of efflux suggests P_i through HvPHT1;6 is cotransported with a net positive charge, therefore HvPHT1;6 is a class of transporter with features in common between a channel and a transporter.

Low-Affinity Transport

HvPHT1;6 showed a linear transport activity for P_i-stimulated inward current over a concentration range of 5 to 30 mM. This concentration range encompasses what the transporter may be exposed to in planta (Schachtman et al., 1998). An apparent linear P_i uptake in a concentration range of 0 to 1 mM can also be interpreted from the data of Rae et al. (2003; Supplemental Material S1) who observed higher P_i influxes in rice suspension cells overexpressing *HvPHT1;6* but with similar K_m to control cells. The linear P_i uptake kinetics in the oocytes matches with the function of the low-affinity P_i transport in barley (*Hordeum vulgare*) leaves (Mimura, 1999) that is required for P_i remobilization.

Stoichiometry of H^+-P_i Cotransport and Speciation

It is widely accepted that P_i uptake in higher plants is coupled to net cation cotransport as P_i absorption depolarizes the plasma membrane of root cortex cells (Mimura, 1999). However, the accurate stoichiometry of X^+-P_i cotransport has not been obtained as yet. By changing the P_i gradients we have demonstrated that when the P_i concentration gradient across the plasma membrane favors higher P_i influx, it produces a larger inward current (Fig. 4). The reversal potentials also shift positive with increasing gradient for inward flux of P_i. We also showed that ^{32}P influx at negative voltages corresponded to the total charge taken up (Fig. 5). Therefore, P_i influx must be coupled with cation influx with a net positive charge entering the cell.

Mammalian P_i transporters are coupled with Na^+ (Bacconi et al., 2005). However, HvPHT1;6 did not use Na^+ or K^+ as a driver cation because the currents induced by P_i and SO_4^{2-} were observed, to the same degree ($P > 0.43$, $n = 7$), in the absence of Na^+ and K^+ in the bath solution (Fig. 7A). On the other hand, pH was found to have a significant effect on the transport activity of HvPHT1;6-expressing oocytes, with the inward tail currents induced by SO_4^{2-} increasing with a decrease in pH. Therefore, H^+ are likely to be the coupling cation to anion movement through

HvPHT1;6. Over the range of pH 6.0 to 8.0, the free concentration of SO_4^{2-} changed less than 0.1 mM (<1% of the total SO_4^{2-} concentration). In contrast, P_i transport increases from pH 6.0 to 7.5 and is reduced at pH 8.0 (Fig. 8B). Because the concentrations of different ionic forms of P_i in solution change with pH, the pH experiment provides evidence that the likely P_i form transported is HPO_4^{2-}. Using the change in inward current with SO_4^{2-} as a function of pH to represent the effect of pH on HPO_4^{2-} transport, we can predict how pH_o should affect inward current, taking into account the change in HPO_4^{2-} with a constant total P_i concentration of 10 mM. This assumes that HPO_4^{2-} and SO_4^{2-} transport behaves the same with pH and that both ions give a linear inward current response with concentration (Fig. 7A). The predicted values show a decrease in inward current with lowered pH as is observed in the experiment. The discrepancy at pH 7 and 6.5 are close to the 95% confidence limits of the measured values and the predicted values from the regression of SO_4^{2-} current as a function of pH. If $H_2PO_4^-$ was the transported ion, the opposite effect would be observed, i.e. a concave-down increase in inward current with decreased pH. Previous work suggested $H_2PO_4^-$ to be the ion transported by HvPHT1;6 (Rae et al., 2003), this however seems very unlikely as discussed above. The HPO_4^{2-} ion, on the other hand, shows a concentration change that aligns with the ionic current responses. Interestingly, $MgHPO_4$ shows a similar concentration change as HPO_4^{2-} with pH. However, $MgHPO_4 + H^+$ is unlikely to be transported through HvPHT1;6 as BAPTA injection reduces active Mg in the oocyte but efflux currents were the same as with no BAPTA injection, and significant influx of P_i (to the same degree, $P > 0.43$, $n = 7$) was observed in the complete absence of Mg^{2+} (Fig. 7A).

Inferences can be made on the transport stoichiometry for H^+-coupled HPO_4^{2-}. A comparison of chemical flux with total ion current from experiments used for Figure 4B gives a ratio of charge to P_i uptake of 1:1, i.e. $3H^+$:1HPO_4^{2-} (calculated on an individual oocyte basis). Radioactive P_i uptake in water-injected oocytes was not significantly different from zero, suggesting an absence of native P_i transporter activities in oocytes under our experimental conditions.

Broad Selectivity of HvPHT1;6

HvPHT1;6 showed little selectivity between HPO_4^{2-} and SO_4^{2-} (Fig. 7A, and radioactive uptake calculations, Figs. 4B and 7B), with a lower transport activity for NO_3^- and Cl^- (Fig. 6A). There was no malate or citrate transport (data not shown). Limited information is available for comparison of anion selectivity in oocytes expressing plant transporters. It has been shown that GmN70, an anion transporter on the symbiosome membrane, favors NO_3^- transport (Vincill et al., 2005), and TaALMT1 favors malate transport but can be selective for Cl^- under certain conditions (Pineros et al., 2008). The HPO_4^{2-} anion has a dehydrated minimum ionic width of 2.518 Å, compared with SO_4^{-2} at 2.535 Å (100.6% of HPO_4^{-2}), NO_3^- at a width of 2.148 Å (84.7% of HPO_4^{-2}), and Cl^- with a width of 1.04 Å (41% of HPO_4^{-2}; ACD/ChemSketch version 11.0, Advanced Chemistry Development, Inc.). SO_4^{-2} is very similar in size and charge density to HPO_4^{-2} (complete hydration of these ions makes HPO_4^{-2} a slightly larger molecule than SO_4^{-2}) and has the same charge and oxyanion characteristics, which seem to be required for selective transport by HvPHT1;6. NO_3^- is also an oxyanion, but is smaller in size, and has only a single negative charge, whereas Cl^- is much smaller and does not have the oxygen. Therefore, the reduced transport of NO_3^- and Cl^- may be expected on this basis. Surprisingly, the electrophysiological experiments did not demonstrate any competition between HPO_4^{2-} and SO_4^{2-} when they were added together and we have shown $^{35}SO_4$ uptake by HvPHT1;6-expressing oocytes without Pi present in the bath. However it does remain a possibility that external SO_4^{2-} may stimulate HPO_4^{2-} transport.

Potential Roles of HvPHT1;6 in P_i Remobilization

P_i is tightly regulated at about 10 mM within plant cell cytoplasm (Schachtman et al., 1998). Nitrate concentration is more variable, between 3.4 to 37 mM (Siddiqi and Glass, 2002). Sulfate in the cytoplasm is at a concentration of approximately 2.5 mM (Cameron et al., 1984). The majority of these anions are removed from senescing leaves. In Arabidopsis (*Arabidopsis thaliana*) 88% of nitrogen, 80% of P, and 68% of S are removed from senescing leaves (Himelblau and Amasino, 2001). *HvPHT1;6* shows the highest expression in the phloem cells of older leaves (Rae et al., 2003). Because HvPHT1;6 shows transport activity of HPO_4^{2-}, SO_4^{2-}, and NO_3^- in oocytes (Fig. 6), it is possibly involved in the remobilization of these ions around the barley plant. Studies have shown rice phloem sap to consist of 8.1 mM PO_4^{3-}, 1.9 mM NO_3^-, and 1.8 mM SO_4^{2-} (Hayashi and Chino, 1985); and wheat (*Triticum aestivum*) phloem sap 8.2 mM PO_4^{3-}, 8.1 mM NO_3^-, and 1.0 mM SO_4^{2-} (Hayashi and Chino, 1986). Therefore, cereals have relatively high levels of these anions remobilized via the phloem. The relatively lower concentration of SO_4^{2-} remobilized could be due to its lower concentration in plant cells (Cameron et al., 1984) and/or its reduced level of removal from senescing leaves (Himelblau and Amasino, 2001), rather than the ability of it to be loaded into the phloem. Remobilization can remove P, S, and nitrogen from older leaves into tissues where it is most needed, in wheat an average 52% to 100% of grain P (Papakosta, 1994) and 72% of grain nitrogen (Gooding et al., 2005) are sourced via remobilization from older plant tissues. It is not entirely clear what significance a low-affinity P_i transporter has in the remobilization of sulfate and nitrate in planta. Further experimentation is warranted; an interesting experiment would be analysis of HvPHT1;6 knockout mu-

tants for differences in remobilization of phosphate, sulfate, and nitrate from senescing leaves.

In summary, nutrient reserves deposited in vegetative plant parts before anthesis buffer grain yield against conditions adverse to assimilation during the grain-filling period. In wheat, remobilization accounts for the majority of grain P content and increases P use efficiency. Phloem tissues are responsible for trafficking nutrient remobilization; and because phosphate, nitrate, and sulfate cannot reach the phloem via the symplast, a transporter must exist in the membranes of barley phloem cells to transport these nutrients into the phloem. We show that HvPHT1;6 is targeted to the plasma membrane of plant cells and has the capacity to transport P_i coupled with protons in a highly voltage-dependent manner. HvPHT1;6 is a low-affinity P_i transporter with potential to transport other oxyanions. HvPHT1;6 could fulfil a role in P_i remobilization because it is highly expressed in phloem tissues. Our results demonstrate that *Xenopus* oocytes can be used for detailed characterization of plant P_i transporters, and this will facilitate structure-function studies of plant P_i transporters.

MATERIALS AND METHODS

Cloning of *HvPHT1;6*

Genomic DNA from barley (*Horedum vulgare* 'Clipper') was used to clone *HvPHT1;6* using PCR with a pair of primers (ATGGCGCGCGAG and TCACACGGGCACCG). PCR products were ligated into the pCR8-GW-TOPO vector (Invitrogen). The resulting *HvPHT1;6* plasmid was sequenced for confirmation, and then *HvPHT1;6* was transferred into a gateway-enabled pGEM-HE-DEST vector (Shelden et al., 2009) using the LR reaction protocol (Invitrogen) for in vitro RNA synthesis. The human *NaPi-IIa* positive control in the KSM expression vector (from Leila Virkki) was digested with *Acc*I and *Hin*dIII, and then cloned into pGEM-HE.

Subcellular Localization of HvPHT1;6::GFP

The coding sequence of *HvPHT1;6* without the stop codon was amplified from *pGEMHvPHT1;6:HE* using the primer pair ATGGCGCGCGAG and CACGGGCACCGTC. The PCR fragment was ligated into the pCR8-GW-TOPO vector, and transferred into *pMDC83* containing the *mGFP* gene (Curtis and Grossniklaus, 2003).The resulting plasmid places *HvPHT1;6* in frame, upstream of *mGFP6*.

Plasmid DNA: CD3-1007 (*AtPIP2A*::*mCherry* fusion), CD3-975 (*γTIP*::*mCherry* fusion), and *pMDC83HvPHT1;6* (5 μg each and 10 μL in total volume) was mixed with 50 μL of 0.6 μm gold particles (Bio-Rad), and bombarded into onion (*Allium cepa*) epidermal cells (900 psi pressure rupture discs) using the Biolostic PDS-1000/He particle delivery system (Bio-Rad). Bombarded onion cells were kept in the dark at room temperature for 48 to 72 h and then examined by the confocal laser-scanning microscopy (Leica TCS SP5 spectral scanning confocal microscope). Onion epidermal cells were grown in Murashige and Skoog medium supplemented with 60 g L^{-1} Suc. The onion epidermal cells were immersed in Murashige and Skoog medium supplemented with 100 g L^{-1} Suc before confocal image analysis. GFP fluorescence was excited using the 488-nm argon laser, and mCherry fluorescence was exited using the 561-nm DPSS 561 laser.

RNA Synthesis

In vitro RNA syntheses were performed on two separate occasions using the T7 RNA polymerase kit (Ambion) for *HvPHT1;6* and *NaPi-IIa*. Synthesis was done at 37°C for 2 h, and the products were cleaned using phenol and chloroform according to manufacturer's instructions. The quality and size of synthesized RNA were checked on RNAse-free agarose gels.

Oocyte Extraction and Preparation

Xenopus laevis frogs (NASCO Biology) were anesthetized in 1 L ice-cold 1.5% (w/v) 3-aminobenzoic acid ethyl ester methanesulfonate salt for 20 min. Oocytes were removed unilaterally from the abdominal cavity, and the lobes were placed in calcium-free Frog Ringer's buffer (in mM: 96 NaCl, 2 KCl, 5 $MgCl_2$, 5 HEPES, pH 7.6). The lobes were cut into small pieces and placed in 50 mL of calcium-free Frog Ringer's buffer containing 100 mg collagenase and 50 mg trypsin inhibitor for 85 to 90 min with rotation on a rotary mixer before being washed three times with hypotonic buffer (in mM: 100 KH_2PO_4 pH 6.5 and 0.1% [w/v] bovine serum albumin). The oocytes were incubated in hypotonic buffer on a rotary shaker for 10 min at room temperature. Oocytes were then washed three times in calcium-free Frog Ringer's, followed by two washes in calcium Ringer's, a 10 min incubation on a rotary shaker, then two washes in calcium Ringer's. The oocytes were maintained at 18°C in MBS solution (in mM): 96 NaCl, 2 KCl, 5 $MgCl_2$, 0.5 $CaCl_2$ 5 HEPES, 10 KH_2PO_4, adjusted to pH 7.6 with KOH; 2.5 mL horse serum was added in 50 mL solution (catalog no. H1270), 50 mg mL^{-1} tetracyclin (5 mg mL^{-1} stock, used 0.5/50 mL), and 0.5 mL per 50 mL of penicillin streptomycin (catalog no. P4333). Healthy stage IV and V oocytes from 10 different oocyte batches were selected for injection with 25 ng RNA (i.e. 50 nL of 500 μg μL^{-1} RNA). The injection into oocyte animal hemisphere was performed at room temperature using a Nanoject II injector (Drummon Scientific Company) and injected oocytes were incubated at 18°C in MBS (replacing daily) for 20 to 96 h prior to ion flux and electrophysiological measurements.

Injection of Phosphate and Nitrate

All chemicals were sourced from Sigma-Aldrich unless stated otherwise. Healthy HvPHT1;6-expressing and water control oocytes (1 d after injection) were selected for injection with 50 nL water (control) or 114 mM NMDG-phosphate (or -nitrate) or 11.3 mM BAPTA, to a final concentration of phosphate (10 ± 0.19 mM) or BAPTA (1 ± 0.02 mM) in the oocyte. These measurements were based on an average (n = 100), and ^3H_2O available internal volume of 570 ± 11 nL (Stegen et al., 2000). After phosphate and nitrate injection, oocytes were incubated at 18°C in MBS for 2 h before electrophysiological measurements.

Solutions

Individual oocytes were selected for voltage clamp experiments. ND-10 bath solution (in mM: 10 NaCl, 80 mannitol, 2 KCl, 1.8 $CaCl_2$, 1 $MgCl_2$, 10 HEPES, and pH 7.5 adjusted with Tris-base) was continuously running at 1.94 mL min^{-1}. This bath solution allowed the addition of up to 30 mM NMDG-phosphate. Solutions adjusted to pH 6 and 6.5 had 10 mM MES instead of HEPES. ND-100 solution was same as ND-10 except that it contained 100 mM NaCl and no mannitol. The BTP solution consisted of 0.3 mM $CaCl_2$ (control), and when varying levels of phosphoric or sulfuric acid were added to the solution, pH was adjusted to 7.5 with BTP. All solutions were adjusted with mannitol to a final osmolarity of 205 mOsmol kg^{-1}.

Electrophysiology

TEVC experiments were performed with a GeneClamp500 amplifier under control of the Clampex8 program (Axon Instruments). Individual experiments were performed on one to six different batches of oocytes and showed exactly the same trend in each occasion. All figures presented in this article were data from oocytes 2 d after injection. Impaling electrodes were filled with 0.22 μm filtered 3 M KCl (0.5–1.0 M current-injecting electrode, and 1.0–2.0 M for voltage-sensing electrode). Oocytes were deemed acceptable if the stable resting membrane potentials were negative of −25 mV in ND-10. The voltage clamp protocol for current tail analysis was 0 mV for 0.5 s, −190 mV for 1 s, −150 mV for 5 s, then a differential voltage ranging 60 mV to −100 mV for 3 s in a −20 mV increment. This protocol was designed so that current activation in *HvPHT1;6*-cRNA-injected oocytes came to a similar saturated level before depolarizing steps.

Phosphate Fluxes

Phosphate influx while simultaneously performing TEVC was measured in ND-10 containing 10 mM NMDG-phosphate. The load solution had $H_3{}^{32}PO_4$

(catalog no. NEX053001MC, Perkin Elmer) added to an average experimental specific activity of 463 cpm nmol^{-1}. A chamber was constructed by indenting the base of a 35 mm diameter petri dish with a soldering iron to hold an individual oocyte. After the oocyte was impaled and TEVC initiated in nonradioactive solution, the solution was immediately replaced with the radioactive solution of an equal phosphate concentration for a 7.5 min voltage clamp at −130 mV. The radioactive solution was immediately replaced by nonradioactive ice-cold solution with 5 × 3 mL washes after the voltage clamp. Scintillation counting was conducted (S6500, multifunction scintillation counter, Beckman and Coulter) on 30 μL of radioactive solution, 30 μL final wash solution with the disintegrated oocyte, and 30 μL final wash solution with 4 mL IRGA-Safe Plus scintillation fluid (Perkin Elmer).

For phosphate efflux measurements, oocytes were incubated in radioactive solution (specific activity of 850 dpm nmol^{-1}) for 24 h at 19°C, and then they were washed for 3 s in 100 μL cold solution. After that, radioactive efflux from oocytes was measured in 100 μL solution at time intervals of 3 s, 5, 10, 20, 40, 80, and 180 min. The remaining radioactivity in oocytes was also measured. Radioactive efflux from water-injected or *HvPHT1;6* cRNA-injected oocytes was also measured in the presence of 10 mM and 0 mM external NMDG-phosphate. A total of 100 μL of each sample was added to 4 mL scintillation fluid for radioactivity counting.

Sulfate Influxes

Sulfate influx was performed exactly the same as phosphate influx, with the exceptions of using 5 mM NMDG-sulfate and a load solution containing $Na_2{}^{35}SO_4$ (catalog no. NEX041H001MC, Perkin Elmer) added to an average experimental specific activity of 3,178 cpm nmol^{-1}.

The HvPHT1;6 nucleotide sequence was deposited in the EMBL database (accession no. FM866444).

Supplemental Data

The following materials are available in the online version of this article.

Supplemental Material S1. Alternative interpretation of P_i uptake when HvPHT1;6 is expressed in rice suspension cells.

Supplemental Material S2. Comparison of HvPHT1;6-induced currents with native oocyte channels.

ACKNOWLEDGMENTS

We thank Dr. Glenn McDonald for useful discussions, and Dr. Sunita Ramesh and Wendy Sullivan for technical assistance and help with ^{35}S experiments. We also thank Leila Virkki for donating the human *NaPi-IIa* positive control in the KSM expression vector.

Received December 6, 2009; accepted December 22, 2009; published January 6, 2010.

LITERATURE CITED

Ai P, Sun S, Zhao J, Fan X, Xin W, Guo Q, Yu L, Shen Q, Wu P, Miller AJ, et al (2009) Two rice phosphate transporters, OsPht1;2 and OsPht1;6, have different functions and kinetic properties in uptake and translocation. Plant J **57:** 798–809

Bacconi A, Virkki LV, Biber J, Murer H, Forster IC (2005) Renouncing electroneutrality is not free of charge: switching on electrogenicity in a Na^+-coupled phosphate cotransporter. Proc Natl Acad Sci USA **102:** 12606–12611

Cameron IL, Hunter KE, Smith NKR (1984) The subcellular concentration of ions and elements in thin cryosections of onion root-meristem cells—an electron-probe eds study. J Cell Sci **72:** 295–306

Curtis MD, Grossniklaus U (2003) A gateway cloning vector set for high-throughput functional analysis of genes in planta. Plant Physiol **133:** 462–469

Daram P, Brunner S, Persson BL, Amrhein N, Bucher M (1998) Functional analysis and cell-specific expression of a phosphate transporter from tomato. Planta **206:** 225–233

Drew MC, Saker LR (1984) Uptake and long-distance transport of phosphate, potassium and chloride in relation to internal ion concentrations in barley—evidence of non-allosteric regulation. Planta **160:** 500–507

Dreyer I, Horeau C, Lemaillet G, Zimmermann S, Bush DR, Rodriguez-Navarro A, Schachtman DP, Spalding EP, Sentenac H, Gaber RF (1999) Identification and characterization of plant transporters using heterologous expression systems. J Exp Bot **50:** 1073–1087

Goldstein AH, Baertlein DA, McDaniel RG (1988) Phosphate starvation inducible metabolism in *Lycopersicon esculentum*. 1. Excretion of acid-phosphatase by tomato plants and suspension-cultured cells. Plant Physiol **87:** 711–715

Gooding MJ, Gregory PJ, Ford KE, Pepler S (2005) Fungicide and cultivar affect post-anthesis patterns of nitrogen uptake, remobilization and utilization efficiency in wheat. J Agric Sci **143:** 503–518

Graham RD, Welch RM (1996) Breeding for Staple Food Crops with High Micronutrient Density. Agricultural Strategies for Micronutrients: Working Paper 3. International Food Policy Research Institute, Washington, DC

Guo B, Jin Y, Wussler C, Blancaflor EB, Motes CM, Versaw WK (2008) Functional analysis of the Arabidopsis PHT4 family of intracellular phosphate transporters. New Phytol **177:** 889–898

Hafke JB, van Amerongen JK, Kelling F, Furch ACU, Gaupels F, van Bel AJE (2005) Thermodynamic battle for photosynthate acquisition between sieve tubes and adjoining parenchyma in transport phloem. Plant Physiol **138:** 1527–1537

Hayashi H, Chino M (1985) Nitrate and other anions in the rice phloem sap. Plant Cell Physiol **26:** 325–330

Hayashi H, Chino M (1986) Collection of pure phloem sap from wheat and its chemical composition. Plant Cell Physiol **27:** 1387–1393

Himelblau E, Amasino RM (2001) Nutrients mobilized from leaves of Arabidopsis thaliana during leaf senescence. J Plant Physiol **158:** 1317–1323

Horst WJ, Abdou M, Wiesler F (1996) Differences between wheat cultivars in acquisition and utilization of phosphorus. Z Pflanz Bodenk **159:** 155–161

Huang CY, Roessner U, Eickmeier I, Genc Y, Callahan DL, Shirley N, Langridge P, Bacic A (2008) Metabolite profiling reveals distinct changes in carbon and nitrogen metabolism in phosphate-deficient barley plants (*Hordeum vulgare L.*). Plant Cell Physiol **49:** 691–703

Jeschke WD, Kirkby EA, Peuke AD, Pate JS, Hartung W (1997) Effects of P deficiency on assimilation and transport of nitrate and phosphate in intact plants of castor bean (*Ricinus communis* L.). J Exp Bot **48:** 75–91

Lambers H, Shane MW, Cramer MD, Pearse SJ, Veneklaas EJ (2006) Root structure and functioning for efficient acquisition of phosphorus: matching morphological and physiological traits. Ann Bot (Lond) **98:** 693–713

Leggewie G, Willmitzer L, Riesmeier JW (1997) Two cDNAs from potato are able to complement a phosphate uptake-deficient yeast mutant: identification of phosphate transporters from higher plants. Plant Cell **9:** 381–392

Liu JY, Versaw WK, Pumplin N, Gomez SK, Blaylock LA, Harrison MJ (2008) Closely related members of the *Medicago truncatula* PHT1 phosphate transporter gene family encode phosphate transporters with distinct biochemical activities. J Biol Chem **283:** 24673–24681

Marschner H, Kirkby EA, Cakmak I (1996) Effect of mineral nutritional status on shoot-root partitioning of photoassimilates and cycling of mineral nutrients. J Exp Bot **47:** 1255–1263

Marten I, Hoth S, Deeken R, Ache P, Ketchum KA, Hoshi T, Hedrich R (1999) AKT3, a phloem-localized K^+ channel, is blocked by protons. Proc Natl Acad Sci USA **96:** 7581–7586

Masoni A, Ercoli L, Mariotti M, Arduini I (2007) Post-anthesis accumulation and remobilization of dry matter, nitrogen and phosphorus in durum wheat as affected by soil type. Eur J Agron **26:** 179–186

Miller AJ, Zhou JJ (2000) Xenopus oocytes as an expression system for plant transporters. Biochim Biophys Acta **1465:** 343–358

Mimura T (1999) Regulation of phosphate transport and homeostasis in plant cells. Int Rev Cytol **191:** 149–200

Mitsukawa N, Okumura S, Shirano Y, Sato S, Kato T, Harashima S, Shibata D (1997) Overexpression of an *Arabidopsis thaliana* high-affinity phosphate transporter gene in tobacco cultured cells enhances cell growth under phosphate-limited conditions. Proc Natl Acad Sci USA **94:** 7098–7102

Molen DT, Breeuwsma A, Boers PCM, Roest CWJ (1997) Dutch Policy Towards Phosphorus Losses in Agriculture. CAB International, Oxon, UK

Morgan MA (1997) The Behaviour of Soil and Fertilizer Phosphorus. CAB International, Oxon, UK

Muchhal US, Pardo JM, Raghothama KG (1996) Phosphate transporters from the higher plant *Arabidopsis thaliana.* Proc Natl Acad Sci USA **93:** 10519–10523

Mudge SR, Rae AL, Diatloff E, Smith FW (2002) Expression analysis suggests novel roles for members of the Pht1 family of phosphate transporters in Arabidopsis. Plant J **31:** 341–353

Nelson BK, Cai X, Nebenfuhr A (2007) A multicolored set of in vivo organelle markers for co-localization studies in Arabidopsis and other plants. Plant J **51:** 1126–1136

Oelkers EH, Valsami-Jones E (2008) Phosphate mineral reactivity and global sustainability. Elements **4:** 83–87

Papakosta DK (1994) Phosphorus accumulation and translocation in wheat as affected by cultivar and nitrogen-fertilization. J Agron Crop Sci **173:** 260–270

Peng ZP, Li CJ (2005) Transport and partitioning of phosphorus in wheat as affected by P withdrawal during flag-leaf expansion. Plant Soil **268:** 1–11

Pineros MA, Cancado GMA, Kochian LV (2008) Novel properties of the wheat aluminum tolerance organic acid transporter (TaALMT1) revealed by electrophysiological characterization in *Xenopus* oocytes: functional and structural implications. Plant Physiol **147:** 2131–2146

Rae AL, Cybinski DH, Jarmey JM, Smith FW (2003) Characterization of two phosphate transporters from barley; evidence for diverse function and kinetic properties among members of the Pht1 family. Plant Mol Biol **53:** 27–36

Schachtman DP, Reid RJ, Ayling SM (1998) Phosphorus uptake by plants: from soil to cell. Plant Physiol **116:** 447–453

Sharpley AN, Chapra SC, Wedepohl R, Sims JT, Daniel TC, Reddy KR (1994) Managing agricultural phosphorus for protection of surface waters—issues and options. J Environ Qual **23:** 437–451

Shelden MC, Howitt SM, Kaiser BN, Tyerman SD (2009) Identification and functional characterisation of aquaporins in the grapevine, *Vitis vinifera*. Funct Plant Biol **36:** 1065–1078

Shenoy VV, Kalagudi GM (2005) Enhancing plant phosphorus use efficiency for sustainable cropping. Biotechnol Adv **23:** 501–513

Shin H, Shin HS, Chen R, Harrison MJ (2006) Loss of At4 function impacts phosphate distribution between the roots and the shoots during phosphate starvation. Plant J **45:** 712–726

Siddiqi MY, Glass ADM (2002) An evaluation of the evidence for, and implications of, cytoplasmic nitrate homeostasis. Plant Cell Environ **25:** 1211–1217

Stegen C, Matskevich I, Wagner CA, Paulmichl M, Lang F, Broer S (2000) Swelling-induced taurine release without chloride channel activity in *Xenopus laevis* oocytes expressing anion channels and transporters. Biochim Biophys Acta **1467:** 91–100

Vincill ED, Szczyglowski K, Roberts DM (2005) GmN70 and LjN70: anion transporters of the symbiosome membrane of nodules with a transport preference for nitrate. Plant Physiol **137:** 1435–1444

Virkki LV, Forster IC, Biber J, Murer H (2005) Substrate interactions in the human type IIa sodium-phosphate cotransporter (NaPi-IIa). Am J Physiol Renal Physiol **288:** F969–F981

Weber WM (1999) Ion currents of *Xenopus laevis* oocytes: state of the art. Biochim Biophys Acta **1421:** 213–233

Weber WM, Liebold KM, Reifarth FW, Uhr U, Clauss W (1995) Influence of extracellular Ca^{2+} on endogenous Cl^- channels in Xenopus oocytes. Pflugers Arch **429:** 820–824